



ELSEVIER

Spectrochimica Acta Part B 56 (2001) 419–430

SPECTROCHIMICA
ACTA
PART B

www.elsevier.nl/locate/sab

The effects of oxygen on the detection of mercury using laser-induced breakdown spectroscopy

R.L. Gleason, D.W. Hahn*

Department of Mechanical Engineering, P.O. Box 116300, University of Florida, Gainesville, FL 32611-6300, USA

Received 13 December 2000; accepted 27 February 2001

Abstract

A systematic study of the processes associated with mercury atomic emission in a laser-induced plasma and the interactions of mercury with oxygen species is presented. At early plasma decay times, on the order of 5–10 μs , no significant variation in mercury atomic emission was observed with the addition of oxygen-containing species. At intermediate and long decay times (10–100 μs), a significant reduction in the 253.7-nm mercury emission intensity was recorded with the introduction of oxygen-containing species. The decrease in mercury emission was temporally coincident with the recombination of atomic oxygen, as measured by the O(I) emission. The decreased mercury emission was not due to thermal effects, based on plasma temperature measurements, and was independent of the molecular source of oxygen, for similar concentrations of oxygen as air, carbon dioxide, and carbon monoxide. Analysis of additional mercury atomic emission lines revealed that the reduction in mercury emission in the presence of oxygen species is limited primarily to the 253.7-nm transition. In concert, the data lead to the conclusion that the 253.7-nm mercury emission line is selectively quenched by oxygen species, primarily O_2 and NO, that are formed during the plasma recombination process. Implications for laser-induced breakdown spectroscopy-based emissions monitoring of mercury species are discussed. © 2001 Elsevier Science B.V. All rights reserved.

Keywords: Laser-induced breakdown spectroscopy; Mercury; Emissions monitoring

1. Introduction

The United States Environmental Protection Agency (US EPA) is preparing to tighten emission standards for many toxic metals, including

arsenic, beryllium, cadmium, chromium, lead and mercury. Although the effects of toxicity drive the regulatory tightening of metal emissions, on-line analytical techniques are currently unable to detect these six toxic metals at concentrations mandated by the new toxicity-based emission standards [1]. Among toxic metals, mercury in particular has received considerable attention due to its high toxicity and its susceptibility to bio-accumulation.

* Corresponding author. Tel.: +1-352-392-0807; fax: +1-352-392-1071.

E-mail address: dwhahn@ufl.edu (D.W. Hahn).

The current US EPA reference method for sampling of toxic metals from gaseous streams has two distinct limitations. First, the sample collection requires collecting and chemically trapping the mercury from the gaseous stream, which may be a function of the mercury species (i.e. vapor, oxides, organo-metal, or particulate-bound). Second, due to the need for sample collection and off-site laboratory analysis, analytical results are often not available for weeks after sample collection. To overcome such limitations, the US EPA has called for the development and use of continuous emission monitors (CEMs) for toxic metals [2]. Current analytical techniques for mercury include spectroscopic methods such as atomic absorption, fluorescence, emission, and mass spectrometry; electrochemical methods and radiometric methods, as well as other common and novel techniques [3]. Although low limits of detection are achieved for a number of the cited techniques, most are not readily implemented for on-line sampling of gaseous streams. In a review of candidate continuous monitoring technologies, the US EPA concluded that more development is required prior to mandating the use of CEMs by hazardous waste combustors [4]. Several candidate CEM technologies were evaluated recently using the exhaust duct of a pilot-scale rotary kiln incinerator in a test sponsored by the US EPA and the US Department of Energy [5]. Although sensitivity and accuracy was achieved for select metals and technologies, no CEM system demonstrated compliance with EPA performance standards for all toxic metals tested, namely Be, Cd, Cr, Pb, and Hg. Nonetheless, the US EPA continues to urge the development and testing of CEMs for toxic metals, which would provide emitting facilities with timely information on emissions, thereby enabling better control and safer facility operation, leading to reduced metals emissions.

Atomic spectroscopy has been used as the basis of mercury detection in a number of systems. Development of multi-metals inductively-coupled plasma (ICP) based CEM systems has been widely studied [6–9]. Thermo Elemental, Franklin, MA, is currently commercializing an ICP-based CEM in cooperation with the US Navy [10]. Development of multi-metals microwave induced plasma

(MIP) CEM systems have also been studied [11–13]. In a recent MIP study, the reduction of emission intensity of the 253.7-nm mercury transition line in the presence of oxygen was noted and investigated by Hadidi et al. [14]. They concluded that the decrease in mercury emission with the addition of oxygen is most likely due to a reduction in the electron impact excitation of mercury. They attributed the more significant reduction in mercury emission in the plasma as compared to other elements in the study (e.g. lead) to the fact that mercury has a very narrow electron impact cross-section compared to the other elements, and is therefore sensitive to small, presumably thermally-induced, changes in electron energy. Hadidi and co-workers did not directly investigate quenching of the mercury signal by oxygen species, although such a mechanism was noted for future investigation.

Laser-induced breakdown spectroscopy (LIBS) offers the potential for real-time analysis of toxic metals at detection limits consistent with proposed US emission standards. LIBS is an atomic emission spectroscopy diagnostic that uses a pulsed laser beam as the excitation source to produce a highly energetic laser-induced plasma (or laser spark). Within the plasma, all species are decomposed into atoms and subsequently excited. The plasma is characterized by emission of a continuum spectrum (bremsstrahlung emission) that also contains discrete atomic emission lines, which result from excitation and recombination of constituents within the plasma. The continuum emission and the discrete atomic emission decay with time, but persist strongly on the order of tens of microseconds. Use of LIBS for mercury detection has been previously reported [15–18]. The general LIBS technique has been widely reported in the literature, and there are a number of literature reviews available [19–21]. Primary advantages of the LIBS technique are the ability to measure concentrations of total mercury, independent of the chemical state, and the suitability of LIBS for in situ, on-line analysis.

In general, LIBS-based detection limits are consistent with US EPA's maximum achievable control technology (MACT) rule requirements for Be, Cd, Cr, and Pb emissions monitoring (5–50

$\mu\text{g}/\text{m}^3$). To date, however, LIBS instrumentation has not been validated and certified by the US EPA or other regulatory agencies as a monitoring technology for regulatory compliance. In contrast, current limits of detection for mercury are generally higher than the proposed emission standard of $40 \mu\text{g}/\text{m}^3$ for new incinerators. Furthermore, when mercury is present in air or oxygen-containing combustion gases, the spectral signal is diminished, and therefore the ability to detect mercury at low concentrations is significantly impacted. The purpose of this study is to develop an understanding of the effect oxygen has on the spectral emission of the 253.7-nm transition line of mercury in a laser-induced plasma. Important mechanisms may include variations in plasma properties (temperature or electron density) in the presence of oxygen, quenching of potential photon energy by oxygen atoms or oxygen-containing species, or the formation of mercury oxide compounds during the plasma decay process.

2. Experimental methodology

2.1. LIBS system apparatus

A Q-switched Nd:YAG laser ($\lambda = 1064 \text{ nm}$) operating with a pulse width of 10 ns, pulse energy of 300 mJ, and 5 Hz pulse rate, was used

as the plasma excitation source for all experiments. The system has been described previously and is summarized here [22]. The laser pulse energy of 300 mJ is significantly above the threshold required for laser-induced breakdown in ambient air (approx. 25–50 mJ per pulse), and was selected to ensure uncoupling of the breakdown process from local matrix effects (e.g. aerosol particle loadings). The apparatus used for the LIBS experiments performed in this paper is provided as Fig. 1.

The plasma emission was collimated using the laser focusing lens, and subsequently diverted from the laser beam path using a 50-mm diameter pierced mirror, launched into a fiber optic cable using a matched 75-mm focal length lens, and coupled to a 0.275-m spectrometer (2400 grooves/mm grating). The plasma emission was recorded using a time-gated, intensified charge-coupled device (ICCD) detector array (1024×256) with an effective linear dispersion of approximately $0.035 \text{ nm}/\text{pixel}$ ($\sim 0.2 \text{ nm}$ spectral resolution). Analog-to-digital conversion was with 14-bit resolution, and the pixel values were converted to wavelength using a linear dispersion and known atomic transition lines for calibration for each 30-nm spectral bandwidth. For this study, the final spectra correspond to the ensemble-average a minimum of 3600 laser pulses, collected in separate 1200–1500 laser pulse sequences.

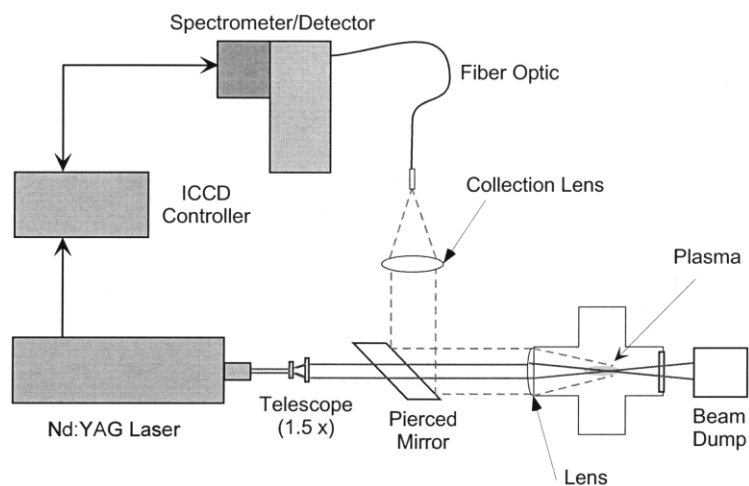


Fig. 1. Schematic of the LIBS system.

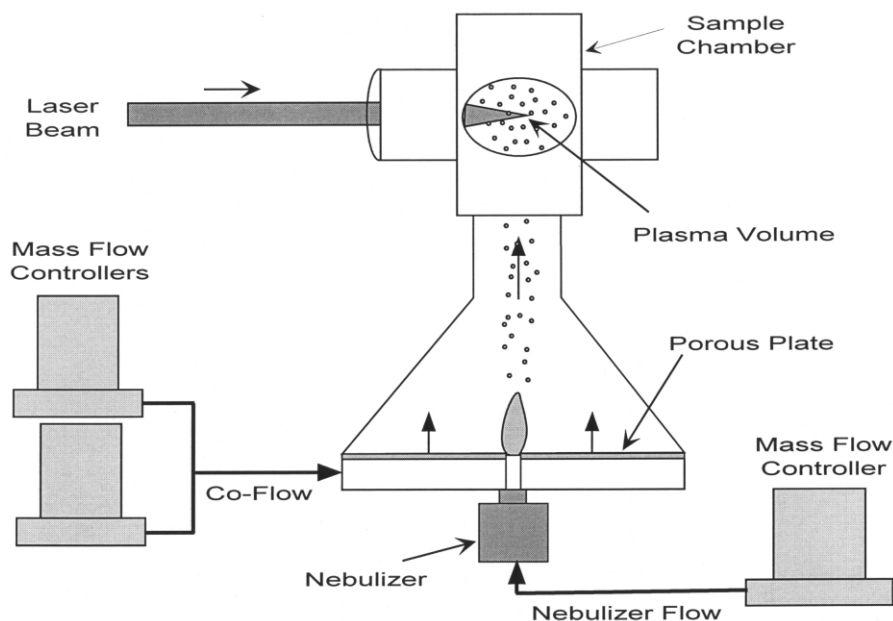


Fig. 2. Schematic of the aerosol source generation system and LIBS sample chamber.

Optical transmission for the entire LIBS system apparatus (lenses, windows, fiber, spectrometer, and detector response) was determined for all relevant wavelengths using a quartz tungsten halogen lamp with calibrated irradiance. The transmission of the apparatus as a function of absolute wavelength and pixel location was determined. Most data are presented as a normalized ratio of analyte peak intensity to baseline intensity, and are therefore independent of absolute transmission. However, as required for plasma temperature determination, the transmission loss of the apparatus was considered for construction of Boltzmann plots.

2.2. Aerosol source generation

An aerosol source apparatus was used to generate particle source streams of mercury or chromium using a typical pneumatic-type medical nebulizer (Hudson Model 1724). The apparatus used to create the particle source stream is illustrated in Fig. 2. Pure nitrogen or air was delivered

to the nebulizer (5 l/min) to induce the aerosol source flow utilizing standard aqueous solutions of the desired analyte. The aqueous solutions were nebulized at a rate of 0.09 ml/min for a corresponding gas flow rate of 5 l/min. Aqueous solutions were prepared from ICP standards (nominal 10000 $\mu\text{g/ml}$ mercury or chromium in 10% nitric acid) and diluted as necessary with ultra-purified deionized water. A uniform carrier gas co-flow stream was developed by passing the co-flow gas through a porous plate, which created an annular flow centered about the nebulizer output. The nebulized aqueous droplets were subsequently dried in the gas stream via evaporation to produce a dispersion of fine, solid particles containing the analyte species. Scanning electron microscopy analyses for a number of generated particles, including beryllium, iron and titanium species, revealed a modal or most probable particle size on the order of 50 nm. By controlling the aqueous solution concentration, nebulization rate, and flow rate of the co-flow gases, the system enables the generation of aerosol source streams at a precise analyte mass concentration. The ana-

lyte concentration in the aerosol stream at the LIBS sample point is given as

$$X = \frac{(\text{Neb. Rate})(\text{Sol. Strength})}{(\text{Co-flow Rate} + \text{Neb. Flow Rate})} \quad (1)$$

where X is the analyte mass concentration in the aerosol flow stream, the Neb. Rate is the mass flow rate of the aqueous solution from the nebulizer, the Sol. Strength is the mass concentration of analyte in the aqueous solution, and the Co-flow Rate and Neb. Flow Rate are the respective gas flow rates. All process flow rates were experimentally verified. A mass concentration of 4850 $\mu\text{g}/\text{m}^3$ was used for the concentration of mercury in the flow stream for the present study. The primary mercury concentration of 4850 $\mu\text{g}/\text{m}^3$ was achieved by nebulizing a solution of 2060 $\mu\text{g}/\text{ml}$ of mercury with 38.3 l/min of total gas flow or by nebulizing a 2500 $\mu\text{g}/\text{ml}$ solution of mercury with a total gas flow of 46.4 l/min. The lower gas flow was used for the molecular oxygen source experiments, and reflects the limiting flow meter capacity for carbon monoxide. The linearity of the 253.7-nm emission line intensity was examined to explore any possible effects from self-absorption at these relatively high mercury concentrations. A linear calibration curve was achieved over the range of mercury concentrations utilized in this study.

2.3. Data collection and processing

Mercury atomic emission was measured as a function of temporal delay following plasma initiation, and as a function of oxygen concentration and the molecular source of oxygen. Except as noted below, mercury data correspond to the 253.7-nm atomic transition line. For all experiments, the emission intensity from each atomic transition line of interest (i.e. absolute peak area) was obtained by summing the intensity over approximately 16 pixels (~ 0.5 nm full width) and then subtracting off the contribution from plasma continuum emission. Baseline subtraction was accomplished by collecting spectra in the presence and in the absence (designated as blank) of the analyte species. Blank spectra were scaled to

match the baseline of the analyte containing spectra using continuum regions on either side of the analyte peak, and the absolute peak intensity of the analyte was calculated from the difference between the analyte-containing and adjusted blank spectra over the pixels centered about the peak. In other cases, blank spectra were not collected, and linear interpolation of the baseline intensity using approximately 30 pixels on either side of the analyte peak was performed to calculate the appropriate baseline. These two methods yielded similar values of the analyte peak intensity, to within 5%, when compared. Final peak-to-base ratios were calculated based on the analyte intensity peak area divided by the baseline continuum emission intensity.

To evaluate the temporal characteristics of mercury emission and the influence of oxygen, spectra were collected at delay times ranging from 5 to 35 μs , using 5- μs increments, with respect to the plasma-initiating laser pulse. A fixed integration time (detector gate width) of 2 μs was used. Subsequent data sets utilized three distinct gating schemes, namely a delay time of 10 μs and an integration time of 10 μs , a delay time of 25 μs and an integration time of 20 μs , and a delay time of 50 μs and an integration time of 150 μs . These three detector gates will be designated as 10/10, 25/20, and 50/150 μs , and correspond temporally to the onset of oxygen effects on mercury emission, and regions of significant oxygen effects, respectively.

Gas matrix effects were investigated by varying the oxygen content from 0 to 20 percent, at 2 percent increments, using a balance of nitrogen. In addition, spectra were collected using flows of pure nitrogen, purified air, a 20% carbon dioxide mixture with a balance of nitrogen, and a 40% carbon monoxide mixture with a balance of nitrogen. The latter two mixtures provided the same nominal concentration of molecular oxygen as found in air.

Plasma temperatures were calculated from the slope of the Einstein-Boltzmann equation using the approach of Corliss and Bozman [23], namely,

$$\ln\left(\frac{\lambda I}{A g}\right) = \left(\frac{1}{T}\right)\left[\frac{-hcE}{k}\right] + \text{const} \quad (2)$$

where A is the transition probability for emission, I is the absolute intensity of the atomic emission line, g is the statistical weight of the excited state, λ is the transition wavelength, E is the upper-level energy of the excited state, h is the Planck constant, c is the speed of light, and k is the Boltzmann constant. The slope of such a plot was used to calculate the plasma temperature. It is noted that this method requires a state of local thermodynamic equilibrium, which is generally considered a valid assumption for times greater than approximately 1 μs following plasma initiation [15]. The plasma was considered optically thin. In addition, a well-spread upper-energy level should be used to increase accuracy [24]. A total of 27 neutral chromium emission lines were measured to construct a Boltzmann plot for temperature calculations. Ensemble-averaging was utilized; hence reported temperatures correspond to the average of thousands of laser pulses. The emission lines ranged from 357.87 nm to 465.21 nm, with a range in upper energy level from 23 305 to 45 663 K. Resulting linear regression coefficients of the Boltzmann plots ranged from 0.96 to 0.98 for all data.

3. Results and discussion

The effect of oxygen (from air) on the mercury 253.7-nm transition line is presented in Fig. 3 as a function of plasma decay time. The data in Fig. 3 are presented as the ratio of the 253.7-nm mercury peak-to-base intensity ratio in air to the mercury peak-to-base intensity ratio in nitrogen. Therefore, a ratio of unity corresponds to no difference in the mercury emission when comparing air and pure nitrogen gas matrices, which is essentially the case for the data recorded at 5 and 10- μs delay times. The mercury emission signal is significantly diminished in the presence of oxygen for delay times greater than approximately 15 μs , as reflected in the marked decrease in the air-to-nitrogen ratios of Fig. 3. For delay times of 30 and 35 μs , the peak-to-base ratio of the mercury emission line in air is reduced fivefold as compared to the value obtained in pure nitrogen, which demonstrates the strong detrimental effect

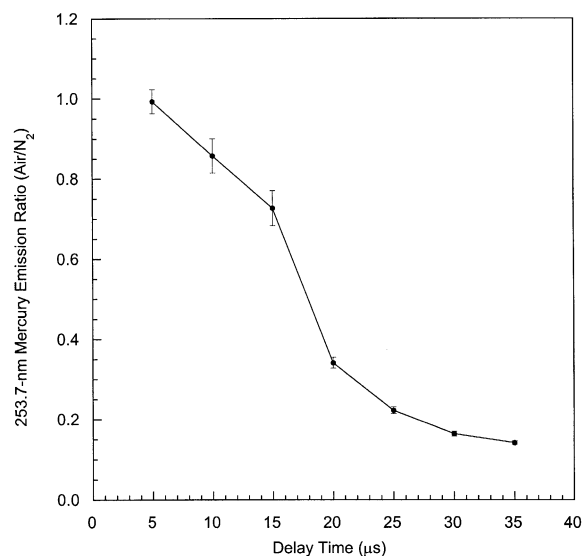


Fig. 3. Ratio of the 253.7-nm mercury emission line peak-to-base intensity ratio in air to the peak-to-base intensity ratio in nitrogen as a function of plasma decay time.

of plasma oxygen on mercury atomic emission intensity.

Data were collected to further quantify the signal reduction of the 253.7-nm mercury transition line as a function of oxygen concentration. The data were collected using a constant detector gating of 25/20 μs , as defined above, which corresponds to the temporal onset of a significant oxygen effect on mercury emission. The percent reduction in the mercury peak-to-base intensity ratio, with respect to the pure nitrogen case, is presented in Fig. 4 as a function of oxygen percentage in the gas matrix. A 50% reduction in normalized mercury emission intensity results from the addition of less than 3% oxygen to the gas stream. With 10% oxygen, the mercury signal is reduced by 75% with respect to the pure nitrogen case, and approaches the 84% reduction observed for 20% oxygen, nominally equal to the baseline case of ambient air. These results demonstrate that a marked reduction in mercury atomic emission is realized with the presence of low concentrations ($\sim 2\%$) of oxygen.

The data presented above elucidate the overall processes associated with mercury atomic emission in a laser-induced plasma and the interac-

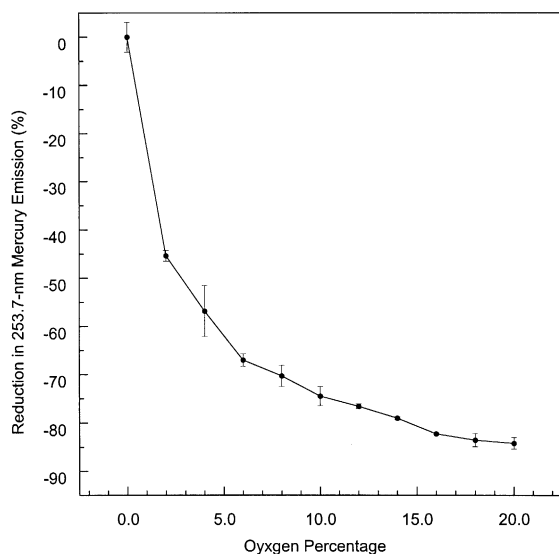


Fig. 4. Percent reduction (with respect to pure nitrogen) in the 253.7-nm mercury emission peak-to-base ratio as a function of O_2 concentration for a detector gate of 25/20 μs .

tions of mercury with oxygen species. At early plasma decay times (on the order of 5–10 μs), plasma temperatures are in excess of 12 000 K and both mercury and oxygen exist primarily as single atoms. Plasma temperature measurements are presented below. Note that all molecular components are initially destroyed via dissociation within the plasma, hence atomic oxygen concentrations are independent of the molecular source of oxygen, as verified in additional experiments discussed below. The current experimental results yield no significant variation in mercury atomic emission during this temporal regime with the introduction of oxygen-containing species; hence, it is concluded that atomic oxygen does not markedly influence mercury atomic emission. At intermediate decay times (i.e. 10–20 μs), the plasma temperature is below 10 000 K and continues to decrease but at a lessened rate. During this period, recombination of atomic oxygen to molecular species, notably O_2 and NO among other species, is initiated and is temporally coincident with a decrease in the 253.7-nm mercury emission intensity. At longer plasma decay times (30–100 μs), it is concluded that nearly all atomic oxygen has recombined and the 253.7-nm mercury signal

is reduced to approximately 10% of the signal levels observed pure nitrogen. More spread among the degree of suppression of mercury emission for various molecular oxygen sources may be expected at lower overall oxygen-equivalent concentrations (e.g. 1%) due to the relatively large gradient of the Fig. 3 plot at low oxygen levels.

Plasma temperature measurements were recorded in both pure nitrogen and air gas streams to explore the possibility of thermal effects on the reduction of mercury emission intensity in the presence of oxygen. The Boltzmann temperatures calculated from the chromium emission lines are summarized in Table 1 for the three distinct temporal regions. The plasma temperatures measured in this study are consistent with values reported in previous studies corresponding to similar plasma conditions [25].

The temperatures of the air and nitrogen plasmas deviate by less than five percent for the 10/10 and 25/20- μs time gates, which is considered to be within the experimental uncertainty of the measurement technique. The temperature difference is approximately 10% for the 50/150- μs time gate, and most likely reflects significant molecular formation at the relatively long delay time, which can lead to variations in the heat capacities of the plasma, as well as different degrees of exothermic/endothermic recombination. Plasma temperatures were not recorded in the current work for the CO or CO_2 cases, due to the interference of a considerable number of molecular lines at the latter two delay times. Nonetheless, the similar plasma temperatures recorded in the air and nitrogen plasmas are consistent with previous investigations and are not expected to vary significantly in the other two gases. Specifically, Yalcin and co-workers reported little varia-

Table 1

Plasma temperature as a function of gas composition for various detector gates

	Pure nitrogen (K)	Purified air (K)
10/10- μs gating	11 320	11 740
25/20- μs gating	9670	9680
50/150- μs gating	9960	8940

tion in laser-induced plasma temperatures and electron densities with changes in gas composition and relative humidity levels [26]. The plasma temperature measurements, in consideration with the Figs. 3 and 4 data, provide strong evidence that thermal effects are not a significant contributor to the mercury atomic emission loss. The absence of thermal effects suggests element-specific interactions between mercury and oxygen species. These element-specific interactions may include quenching of the mercury 253.7-nm transition energy by elemental or molecular oxygen species, or formation of mercury oxide molecules (e.g. HgO or HgO₂) during the transient plasma decay process.

During initial plasma formation, all species and fine particulates are decomposed into either neutral or ionized atoms, hence oxygen exists as atomic oxygen and all information from the molecular source of oxygen is lost. To investigate any influence of the molecular source of oxygen, measurements were recorded utilizing similar concentrations of molecular oxygen, nominally 20% O₂, from gas matrices composed of air, carbon dioxide, or carbon monoxide. Representative spectra for these three carrier gases along with a spectrum corresponding to pure nitrogen are presented in Figs. 5 and 6 for the 10/10 and 25/20- μ s detector gates, respectively. For the relatively short delay time of 10 μ s, the intensity of the mercury emission peak is similar in all four spectra, which is consistent with the air and nitrogen results presented in Fig. 3. The Fig. 5 spectra are similar for all three oxygen-equivalent carrier gases, namely air, carbon monoxide, and carbon dioxide, which corroborates the concept of complete molecular dissociation within the plasma. The mercury peak-to-base ratios for all carrier gases are quantified below. In contrast to the 10/10- μ s results, the spectra corresponding to the detector gate of 25/20- μ s are characterized by a similar marked reduction in the intensities of the mercury emission line in the three oxygen-containing gas streams as compared with the intensity of the mercury emission line in a pure nitrogen atmosphere. A similar trend was recorded for the 50/150- μ s detector gate. It is also noted that several additional emission lines

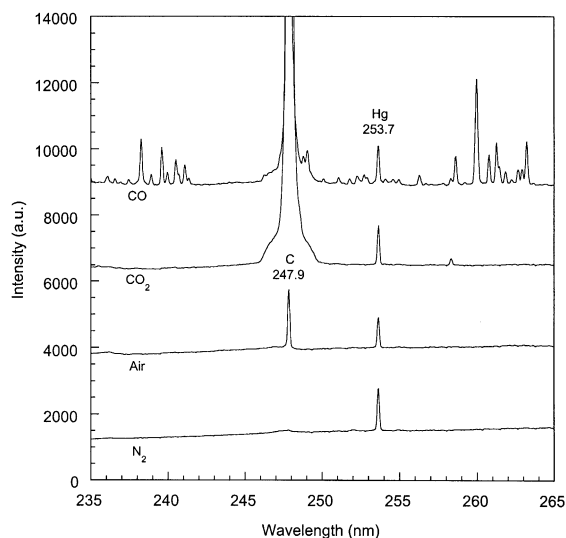


Fig. 5. LIBS emission spectra for four different gas streams for a detector gate of 10/10 μ s. All spectra have the same intensity scale but have been shifted for clarity.

are visible in Figs. 5 and 6 for the CO gas stream. These features were also observed with the 50/150- μ s detector gate, and are attributed to CO emission bands (namely A¹ Π \rightarrow X¹ Π) resulting from the excitation of CO molecules on the perimeter of the plasma [27].

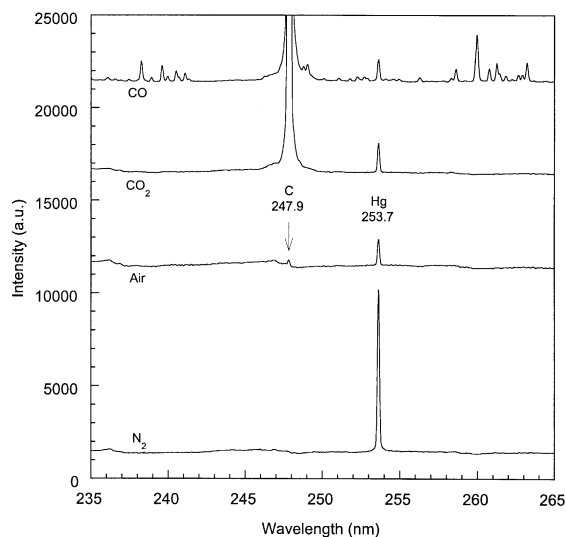


Fig. 6. LIBS emission spectra for four different gas streams for a detector gate of 25/20 μ s. All spectra have the same intensity scale but have been shifted for clarity.

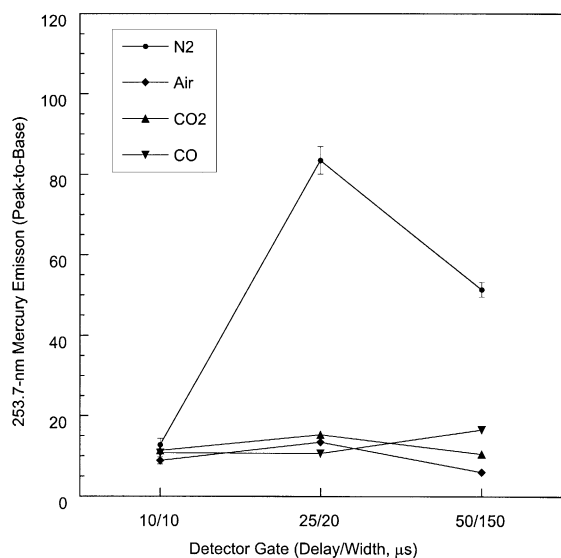


Fig. 7. Peak-to-base intensity ratio of the 253.7-nm mercury emission line as a function of detector gating for four different gas streams.

To quantify the above results, the peak-to-base ratios were evaluated for all four carrier gasses (pure nitrogen, air, 20% carbon dioxide, and 40% carbon monoxide) and for all three detector gates (10/10 μ s, 25/20 μ s and 50/150 μ s). The peak-to-base ratios for all cases are presented in Fig. 7. For the 10/10- μ s detector gate, all four gas streams yield similar mercury emission intensities, although the three oxygen-containing streams correspond to a modest reduction in mercury emission intensity ranging from 10 to 30%, with respect to the pure nitrogen values. The reductions are consistent with the temporal data presented in Fig. 3, and are noted to correspond to a temporal integration from 10 to 20 μ s. Because the absolute plasma emission intensity decreases nonlinearly with time, the temporal integration is weighted strongly to the shorter delay times, hence only the approximate 20% reduction. Due to near complete molecular dissociation in the plasma at early times, the data suggest that atomic oxygen has no apparent effect on the mercury 253.7-nm transition line emission at short delay times. Additional results reported below support the presence of significant atomic oxygen during the 10/10- μ s gate.

For the 25/20- μ s and 50/150- μ s detector gates, the presence of oxygen-containing species yielded a significant reduction on the mercury emission intensity in comparison to the pure nitrogen results. For the 25/20- μ s gate, the mercury emission line peak-to-base ratio was reduced from 83.5 in pure nitrogen to values of 13.5, 15.3 and 10.7 in the air, 20% carbon-dioxide, and 40% carbon monoxide gas streams, respectively. Similar results were observed for the 50/150- μ s gate. For the 25/20- μ s data, the peak-to-base ratio for the mercury transition line was approximately six times larger in nitrogen than that in the O₂, CO₂, and CO-containing carrier gases. The O₂, CO₂, and CO-containing gas streams resulted in nominally equal peak-to-base ratios, approximately $13.2 \pm 20\%$. The data indicate that the presence of oxygen-containing species has a strong effect on the mercury 253.7-nm transition line emission at intermediate to long plasma decay times. Furthermore, the oxygen effect is essentially independent of the molecular source of oxygen in the plasma, consistent with the complete dissociation of all molecular species during the initial plasma formation. Although all atomic oxygen is not expected to recombine to the same species irrespective of the molecular source, significant O₂ and NO are expected to form from air, carbon dioxide, or carbon monoxide gas streams. Thermodynamic considerations during plasma recombination are the subject of future investigation. Nonetheless, as observed in the Fig. 4 data, recombination of only 10–20% of the available oxygen atoms is sufficient to suppress the mercury emission to levels comparable to the air results, hence independence of the molecular source of oxygen at oxygen concentrations equivalent to ambient air.

The strong correlation of temporal and gas matrix effects suggests that the recombination of atomic species, namely the formation of diatomic oxygen or other oxygen compounds, or perhaps mercury oxide species, is responsible for the reduction in mercury emission. To further elucidate such phenomena, additional experiments were performed to monitor the recombination of atomic oxygen. No suitable diagnostic schemes were available to directly detect the temporal

evolution of diatomic oxygen within the plasma. Alternatively, the evolution of atomic oxygen, O(I), was used as an indicator for the recombination of atomic oxygen. The intensity of three atomic transition lines of neutral atomic oxygen, namely at wavelengths of 394.73 nm, 394.75 nm and 394.76 nm, were measured as a function of plasma decay time. The three peaks were not resolved spectrally, and the data were processed using a single peak-to-base ratio for the O(I) triplet. The peak-to-base ratio of the atomic oxygen emission peak as a function of plasma decay time is presented in Fig. 8. A marked decrease in O(I) emission occurs at a plasma decay time of 15 and 20 μs . For longer decay times, the O(I) emission intensity remains diminished, and is gone completely by approximately 30 μs . In consideration with the relatively minor slope of the temporal evolution of plasma temperature (see Table 1 data), it is concluded that the demise in atomic oxygen emission is due to atomic oxygen recombination rather than a reduction in excitation of atomic oxygen. Detailed equilibrium modeling of the nitrogen-oxygen plasma system is desirable to confirm the recombination dynamics of O(I) and O_2 . It is noted that the calculated equilibrium concentrations of O_2 in oxygen and water vapor plasmas show highly non-linear increases with decreasing plasma temperature in the temperature range of current interest [28].

The data presented above suggest that the observed reductions in mercury atomic emission in the presence of oxygen-containing species are related to the recombination of atomic oxygen. To illustrate the temporal correlation of the suppression of mercury emission and the recombination of atomic oxygen, the Fig. 3 data are added as an overlay to O(I) emission data presented in Fig. 8. Significantly, the demise in mercury emission is in near perfect correlation with the recombination of atomic oxygen, presumably to form diatomic oxygen among other species. It is proposed that the reduction in mercury emission is the result of quenching of the 253.7-nm transition energy by molecular oxygen species, namely O_2 or NO, although the formation of mercury oxide molecules during oxygen recombination could also contribute to such a signal reduction. To elimi-

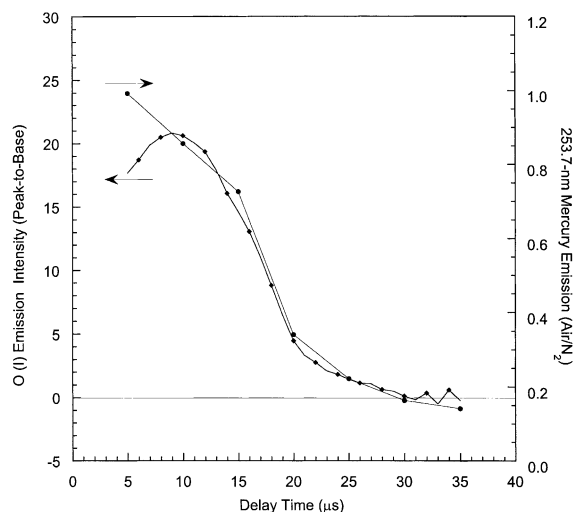


Fig. 8. Peak-to-base intensity ratio of the O(I) emission triplet in air as a function of plasma decay time. Fig. 3 data are included for comparison.

nate this latter mechanism, additional measurements were recorded utilizing additional mercury atomic emission lines.

The mercury atomic emission intensities corresponding to the wavelengths 253.7 nm, 365.02 nm and 435.83 nm were measured in both nitrogen and in purified air using the 10/10- μs and 25/20- μs detector gates. To increase the overall emission intensity of the latter two lines, the mercury concentration was increased to 19 400 $\mu\text{g}/\text{m}^3$ for these experiments. For the 25/20- μs detector gate, the peak-to-base ratio of the 253.7-nm emission line was decreased by 89.5% from pure nitrogen to purified air, which is consistent with the above results. The peak-to-base ratios corresponding to the 365.02 and 435.83-nm emission lines both decreased by only 18.1% from the pure nitrogen to purified air gas streams. This fivefold difference in signal reduction between the various mercury emission lines indicates that the mercury atomic emission signal loss is specific to the 253.7-nm transition line. These results suggest that the formation of mercury-oxide molecules are not a contributing factor to the observed decrease in mercury atomic emission, because the loss of a mercury atom to mercury oxide formation would

produce a corresponding reduction in all mercury transition lines due to the loss of an emitting mercury atom. In concert, the above results provide strong evidence to support the transition-specific quenching of the 253.7-nm line, most likely by oxygen-containing species, subsequent to molecular recombination within the plasma. To provide further evidence of emission quenching, a Stern–Volmer plot ($I_{253.7}^{-1}$ vs. $[O_2]$) was constructed. Consistent with emission quenching, the plot was highly linear, with a regression coefficient of 0.996.

The finding that the marked reduction in mercury atomic emission in the presence of oxygen is limited primarily to the 253.7-nm transition is consistent with the conclusion of selective molecular quenching of this transition energy, rather than the loss of mercury atoms to molecular recombination (e.g. mercury oxide). There is little recent literature on the quenching of mercury atomic emission by molecular species, however, several comprehensive literature reviews were published in the 1960s [29–31]. Detailed studies report quenching cross-sections of the 253.7-nm mercury transition ($6^3P_1 \rightarrow 6^1S_0$) for a number of species, including H_2 , O_2 , NO , CO_2 , N_2O and N_2 [32–34]. The quenching cross-sections of O_2 and NO are comparable, and are significantly larger than the values reported for the other molecules. Specifically, the quenching cross-section of O_2 is 5 times larger than the cross-section of CO_2 and nearly two orders of magnitude larger than the value of N_2 . Because both O_2 and NO molecules are formed during plasma recombination, it is concluded that the reduction in 253.7-nm mercury emission is most likely due to quenching by these two species.

4. Conclusions

This study has demonstrated that the LIBS-based analysis of the 253.7-nm mercury atomic transition is affected by the presence of oxygen species. Based on plasma temperature measurements, thermal effects are not responsible for the

observed signal reduction. Furthermore, the reduction in mercury emission is essentially independent of the molecular source of oxygen, at equivalent ambient air O_2 levels, which is consistent with the well-established process of complete molecular dissociation within energetic laser-induced plasmas. The temporal profiles of 253.7-nm mercury emission data and atomic oxygen emission data, combined with the investigation of additional mercury emission lines, lead to the conclusion that the 253.7-nm mercury emission line is selectively quenched by oxygen species, primarily O_2 and NO , formed by recombination of atoms during the plasma decay process. Because the 253.7-nm emission line is the strongest mercury emission line in laser-induced plasmas, the effects of oxygen have implications on the development and calibration of LIBS-based real-time emissions monitors. For example, effluent streams from incinerators are subject to varying levels of oxygen, primarily as diatomic oxygen and carbon dioxide. The present work suggests several solutions to real-time monitoring problems, such as the use of temporal gating to limit mercury emission detection to relatively early temporal regimes where the potential effect of molecular quenching is mitigated by the presence of atomic oxygen. A drawback of such an approach is that the optimal detector gating for mercury detection corresponds to longer delay times, as observed in the peak-to-base ratios of Fig. 7. In addition, short delay times may not be consistent with other analyte lines necessary for multi-metals monitoring. An additional approach is to optimize the LIBS detection scheme temporally, and then develop a calibration scheme to correct for the deviation of total oxygen about some nominal calibration value. On-line O_2 and/or CO_2 sensors are generally employed on most thermal treatment facilities, hence total oxygen data should be readily available as an input to advanced data reduction algorithms. Overall, it is hoped that an increased understanding of the interactions between plasmas and metal species will facilitate advancement of the present state of real-time monitors targeted to metal species such as mercury.

Acknowledgements

The authors gratefully acknowledge Brian Fisher for assistance with measurements, and Ben Smith (Department of Chemistry) for useful discussions. This work was supported in part by the US Department of Energy and US Department of Defense, Joint Services Demil Technology Office, in conjunction with Sandia National Laboratories.

References

- [1] N.B. French, W. Haas, S. Priebe, *Spectroscopy* 15 (2000) 24–32.
- [2] US Environmental Protection Agency, Fed. Register 61 (77) (1996) 17357–17358.
- [3] W.L. Clevenger, B.W. Smith, J.D. Winefordner, *Crit. Rev. Anal. Chem.* 27 (1997) 1–26.
- [4] US Environmental Protection Agency, Fed. Register 62 (249) (1997) 67788–677818.
- [5] P.M. Lemieux, J.V. Ryan, N.B. French, W.J. Haas, S. Priebe, D.B. Burns, *Waste Manage.* 18 (1998) 385–391.
- [6] D. Nore, A.M. Gomes, J. Bacri, J. Cabe, *Spectrochim. Acta Part B* 48 (1993) 1411–1419.
- [7] C.C. Trassy, R.C. Diemiaszonek, *J. Anal. At. Spectrosc.* 10 (1995) 661–669.
- [8] A.M. Gomes, J.P. Sarrette, L. Madon, A. Almi, *Spectrochim. Acta Part B* 51 (1996) 1695–1705.
- [9] M.D. Seltzer, G.A. Meyer, *Environ. Sci. Technol.* 31 (1997) 2665–2672.
- [10] M.D. Seltzer, *J. Air Waste Manage.* 50 (2000) 1010–1016.
- [11] V. Siemens, T. Harju, T. Laitinen, K. Larjava, J.A.C. Broekaert, *Fresenius J. Anal. Chem.* 351 (1995) 11–18.
- [12] Y. Duan, S. Yongzuan, Z. Jin, *Anal. Chem.* 72 (2000) 1672–1679.
- [13] P.P. Woskov, D.Y. Rhee, P. Thomas, D.R. Cohn, J.E. Surma, C.H. Titus, *Rev. Sci. Instrum.* 67 (1996) 3700–3707.
- [14] K. Hadidi, P.P. Woskov, G.J. Flores, K. Green, P. Thomas, *Jpn. J. Appl. Phys.: Part 38* 1 (1999) 4596–4600.
- [15] L.J. Radziemski, T.R. Loree, D.A. Cremers, N.M. Hoffman, *Anal. Chem.* 55 (1983) 1246–1252.
- [16] M. Casini, M.A. Harith, V. Palleschi, A. Salvetti, D.P. Singh, V. Vaselli, *Laser Particle Beams* 9 (1991) 633–639.
- [17] C. Lazzari, M. DeRosa, S. Rastelli, A. Ciucci, V. Palleschi, A. Salvetti, *Laser Particle Beams* 12 (1994) 525–530.
- [18] H. Zhang, F.Y. Yuen, J.P. Singh, *Appl. Optics* 38 (1999) 1459–1466.
- [19] D.A. Rusak, B.C. Castle, B.W. Smith, J.D. Winefordner, *Crit. Rev. Anal. Chem.* 27 (1997) 257–290.
- [20] I. Schechter, *Rev. Anal. Chem.* 16 (1997) 173–298.
- [21] K. Song, Y.I. Lee, J. Sneddon, *Appl. Spectrosc. Rev.* 32 (1997) 183–235.
- [22] D.W. Hahn, M.M. Lunden, *Aerosol Sci. Technol.* 33 (2000) 30–48.
- [23] C.H. Corliss, W.R. Bozman, *Experimental Transition Probabilities for Spectral Lines of Seventy Elements*; National Bureau of Standards Monograph 53, United States Department of Commerce, Washington, DC, 1962 (Ch. 1).
- [24] C.A. Bye, A. Scheeline, *Appl. Spectrosc.* 47 (1993) 2022–2030.
- [25] M. Essien, L.J. Radziemski, J. Sneddon, *J. Anal. At. Spectrom.* 3 (1988) 985–988.
- [26] S. Yalcin, D.R. Crosley, G.P. Smith, G.W. Faris, *Frennius J. Appl. Phys. B: Laser Optics* 68 (1999) 121–130.
- [27] R.W.B. Pearse, A.G. Gaydon, *Identification of Molecular Spectra*, Wiley, New York, 1963.
- [28] W. Lochte-Holtgreven, *Plasma Diagnostics*, American Institute of Physics, Woodbury, NY, 1995.
- [29] H.E. Gunning, O.P. Strausz, *Adv. Photochem.* 1 (1963) 209–274.
- [30] R.J. Cvetanovic, *Progress React. Kinet.* 2 (1964) 39–130.
- [31] J.G. Calvert, J.N. Pitts, Jr., *Photochemistry*, Wiley, New York, 1966.
- [32] J.S. Deech, J. Pitre, L. Krause, *Can. J. Phys.* 49 (1971) 1976–1981.
- [33] J.V. Micheal, G.N. Suess, *J. Phys. Chem.* 78 (1974) 482–487.
- [34] S.D. Gleditsch, J.V. Michael, *J. Phys. Chem.* 79 (1975) 409–413.